Lung Deposition of Airborne Particles – Resolved in a Single Breath

Amalia Larsson Hurtig

DIVISION OF ERGONOMICS AND AEROSOL TECHNOLOGY | DEPARTMENT OF DESIGN SCIENCES
FACULTY OF ENGINEERING LTH | LUND UNIVERSITY
2020

MASTER THESIS

Lung Deposition of Airborne Particles – Resolved in a Single Breath

Amalia Larsson Hurtig

LUND
UNIVERSITY

Lung Deposition of Airborne Particles – Resolved in a Single Breath

Published by
Department of Design Sciences
Faculty of Engineering LTH, Lund University
P.O. Box 118, SE-221 00 Lund, Sweden

Subject: Aerosol Technology (MAMM05)
Division: Ergonomics and Aerosol Technology
Supervisor: Jenny Rissler
Co-supervisor: Jakob Löndahl
Examiner: Anders Gudmundsson

Abstract

Exposure to airborne particulate matter has been declared to cause cardiovascular and respiratory disease as well as cancer. By understanding how the aerosol particles deposit in our respiratory tract, we can understand how the exposure to airborne particles affect our health. The health effects partly depend on which type of particles that we are exposed to, but also how sensitive we are as individuals. In this thesis a set-up was built for studying the airborne particles in the breathing zone, with time resolution in each breath. The set-up was developed after investigating previous set-ups in literature and consists of three main modules, i.e. an aerosol generation module, an inhalation system and a particle detection unit. The stability and output of different nebulizers were tested, the breathing-flow module was calibrated, and the inhalation system was designed and 3D-printed. The final set-up was designed to minimize losses and allow for spontaneous breathing. A fast CPC was used to characterize the final set-up for abrupt flow changes and also for a realistic breathing pattern of an adult, generated by a breathing simulator. The CPC showed a proof of concept with respect to the time resolution requirements for the designed set-up. However, due to fluctuations in the CPC sample flow during high inhalation and exhalation flowrates there is a need for a more reliable and stable measurement device with high time resolution before using the suggested set-up in real lung deposition studies.

Keywords: Aerosols, Airborne particles, Inhalation, Lung deposition, Respiratory tract deposition

Sammanfattning

Exponering av luftburna partiklar har utpekats som orsak till hjärt- och kärlsjukdomar, luftvägssjukdomar samt cancer. Genom att förstå hur aerosoler deponeras i våra luftvägar och lungor kan vi förstå hur exponeringen av luftburna partiklar påverkar vår hälsa. Hälsoeffekterna beror delvis på vilken typ av partiklar som vi utsätts för, men också hur känsliga vi är som individer. I det här examensarbetet har en uppställning byggts för att kunna studera luftburna partiklar i andningszonen, med tidsupplösning i varje andetag. Uppställningen designades efter att ha studerat tidigare uppställningar i litteraturen och består av tre huvudmoduler, en aerosolgenereringsmodul, ett inhalationssystem och en enhet för partikeldetektion. Stabiliteten av aerosolgenereringen testades för olika nebulisatorer, flödesmodulen kalibrerades och inhalationssystemet designades och 3D-printades. Den slutliga uppställningen är designad för att minimera förluster och tillåta spontan andning. En snabb CPC användes för att karaktärisera den slutliga uppställningen för abrupta flödesändringar och även för ett realistiskt andningsmönster som genererades av en artificiell lunga. CPCn fungerade som konceptvalidering gällande tidsupplösningskravet. Dock framkom det att CPCn hade ett fluktuerande samplings-flöde för höga andningsflöden. På grund av detta behövs ett mer robust och pålitligt mätinstrument med hög tidsupplösning innan den framtagna uppställningen kan användas i lungdeponeringsstudier.

Nyckelord: Aerosol, Luftburna partiklar, Inhalation, Lungdeponering

Acknowledgments

This thesis was performed during the fall of 2019 at the Ergonomics and Aerosol Division, Department of Design Sciences at the Faculty of Engineering, Lund University as part of the program Engineering Nanoscience - Nanophysics.

First of all, I would like to thank my supervisors, **Jenny Rissler** and **Jakob Löndahl**, for all their time, support and guidance. They introduced me to the world of aerosols and how it is to build your own test equipment.

Furthermore, I would like to thank:

Julia Dobric and **Karin Lovén**, for helping me out in the lab and also when analysing the first aerosol generation data.

Patrik Nilsson, for helping with purchases, operating the equipment in the lab as well as soldering the electronics.

Bert Berglund, for milling a metal box for my pressure sensor to be fixated in.

Mårten Svensson and **Peter Elfman** at Emmace Consulting, for lending out the artificial lung.

Last but not least, I would like to thank the whole aerosol group for creating such an inspirational, sharp and supportive climate to be part of.

Lund, January 2020

Amalia Larsson Hurtig

Table of Contents

List of Acronyms and Abbreviations

AMS	aerosol mass spectrometer
APS	aerodynamic particle sizer
CPC	condensation particle counter
DAQ	data acquisition card
DMA	differential mobility analyzer
DPI	dry-powder inhaler
HEPA	high efficiency particulate arresting (filter)
IKDC	Ingvar Kamprad Designcentrum
lpm	liters per minute
MCPC	mixing condensation particle counter
NaCl	sodium chloride
$(NH_4)_2SO_4$	ammonium sulphate
OPS	optical particle sizer
PSL	polystyrene latex
Re	Reynolds number
RH	relative humidity
SMPS	scanning mobility particle sizer
SiO_2	silicon dioxide
V_t	tidal volume
WHO	World Health Organization

1 Introduction

This section introduces the reader to the research problem investigated in this thesis and provides a background that puts the research into a societal perspective.

1.1 Background

The number of urban sources that release airborne particles into the air has seen a considerable increase over the years. Exposure to air pollution has been listed as a key issue in terms of health by the World Health Organization (WHO) (World Health Organization, 2018). WHO states that PM2.5 (particulate matter of 2.5 µm or less in diameter) is a cause of cardiovascular and respiratory disease as well as cancer (World Health Organization, 2018). By understanding how airborne particles are deposited in our lungs, we can understand how the exposure to air pollutants and other airborne particles affect our health. It is only the fraction of particles that get caught in the lungs that will give rise to the health effects. These potential health effects will partly depend on which type of particles (material, size etc.) that we are exposed to, but also how sensitive we are as individuals. The outdoor air quality depends heavily on where we are situated - in a city there are many particle sources whereas in the countryside there are fewer. One important factor for the individual sensitivity to airborne particles and air pollutants is the individual variance in how the particles deposit in the lungs (Rissler et al. 2017b). It has been shown that the deposition varies a lot from individual to individual (Rissler et al. 2017a). Thus, it is of outermost interest to study how many particles that deposit in the lungs and where the deposition occurs. Respiratory tract deposition has been researched for over a decade at the aerosol-group at LTH with various measurements. The next step is to study the deposition online, within a single breath. Such a set-up would enable a deeper understanding of at which lung-depth the particles deposit. Furthermore, the set-up would facilitate for faster collection of lung deposition data from different groups of individuals (healthy, diseased, young, old, man, woman etc.) without posing any health risk itself.

1.2 Purpose

This thesis aims to build and test a novel set-up capable of detecting airborne particles in the breathing zone, with time resolution in each breath. The project is a continuation of previous and ongoing research at the aerosol group, within the area of measuring respiratory tract deposition of airborne particles. Suggested schematic drawings and ideas for the set-up of the system already existed at the start of this work, thus the work has focused on refining the suggested set-up, building and performing first measurements.

By setting up a system and performing first measurements of the particle lung deposition the aim is to study the fast variance in concentration at the breathing zone for a well-defined aerosol during inhalation and exhalation. The detection of particles will be made using optical instruments.

1.3 Research Questions

The thesis aims to answer the following main research question in order to fulfill its purpose presented above:

- How can we build a set-up for studies of particle lung deposition with time resolution in each breath?

With respect to the main research question, several supporting questions were formulated that supports the main question.

- What set-ups are used for lung deposition measurements today?
- What design parameters and instruments are needed to fulfill the time requirements?
- What aerosol particle types would be suitable for lung deposition studies in the suggested set-up?

2 Theory

This section presents the theoretical background of aerosols, including the physicochemical properties, common measurement techniques and respiratory tract deposition.

2.1 Aerosols

An aerosol is defined as an assembly of solid or liquid particles (particle size generally about 1 nm - 100 µm) suspended in a carrier gas, most commonly air (Kulkarni, Baron & Willeke, 2011). Aerosols occur naturally in our surroundings, e.g. as dust, fog etc., they are also produced and released during industrial processes such as combustion. Furthermore, aerosols can also be created and manufactured in the lab. The shape of airborne particles ranges from ideally shaped spheres to more complex shapes such as fibers, aggregates and crystalline particles with sharp edges or fractured surfaces. To characterize and investigate the properties of different aerosols it may be of interest to study their chemical composition, surface area, mass and particle diameter. There are several techniques and instruments used to gather valuable information about airborne particles. When looking at the health effects and toxicity of aerosols entering the lung there are several properties that influence the deposition rate in the lung. These properties include diffusion, impaction, gravitational settling and interception, properties that are related to the particle size. When particles have already been deposited, other properties such as surface area and chemistry are important for investigating how the particles may interact with the tissue in the lung. Research within respiratory tract deposition of aerosols, (e.g. Löndahl et al. 2014; Heyder et al. 1973 & Lin et al. 2019) frequently uses monodisperse aerosols for studying the deposition in the lungs. In a monodisperse aerosol, all particles are of the same size, or a small range of sizes. Monodispersity may be an advantageous property when studying inhaled aerosols as it reduces the complexity and allows for measurement of particles counts only and one may exclude size characterization at the high time resolution needed (Heyder et al. 1973).

2.1.1 **Particle Motion and Deposition**

Particles in different size ranges behave differently and are governed by different physical laws (Kulkarni, Baron and Willeke, 2011). Fluid motion for objects of different sizes is often described in terms of the forces that are present. The flow pattern of the gas is described by the ratio between the inertial force of the gas and the friction force of the gas moving over the surface. This ratio is illustrated by the Reynolds number (Re):

$$Re = \frac{\rho_g V d}{\eta} = \frac{V d}{\nu} \tag{2.1}$$

where d is a characteristic dimension of the object, V is the gas velocity, ν is the kinematic viscosity ($=\eta/\rho_g$), η is the gas viscosity and ρ_g is the gas density. The Re characterizes the flow, meaning the gas and not the particles themselves. There is a distinction between the flow Re and the particle Re. At low Re, friction forces are dominating and the flow is laminar. Under these circumstances, there are no streamlines that loop back on themselves. For higher Re, the inertial forces become more prominent and loops start appearing. At an even higher Re the flow eventually becomes turbulent. (Kulkarni, Baron & Willeke, 2011)

In a cylindrical tube, the friction at the wall will slow down the velocity of the gas relative to the movement at the center of the tube. This friction force produces a laminar parabolic velocity profile at low Re, see Figure 2.1.

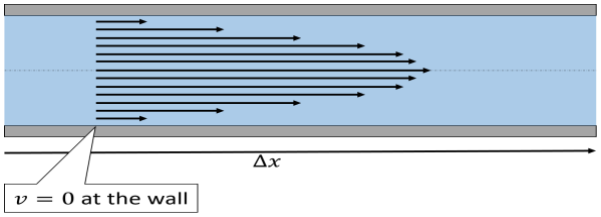

Figure 2.1 Schematic drawing of the laminar flow velocity profile in a tube.

2.1.1.1 Thermodynamic Domain

Diffusion, also referred to as Brownian motion, is defined as the random movement of particles or molecules in a gas, initiated by a concentration gradient (Kulkarni, Baron & Willeke, 2011). The diffusivity is computed as follows:

$$D = \frac{k\,T\,C}{3\,\pi\,\eta\,d_p} = k\,T\,B \tag{2.2}$$

where k is the Boltzmann constant, T is the temperature, B is the mechanical mobility, C is the slip correction factor, d_p is the particle diameter and η is the gas

viscosity. As shown in Equation 2.2 small particles will diffuse faster than large particles. (Kulkarni, Baron & Willeke, 2011)

2.1.1.2 Aerodynamic Domain

For larger particles, with a diameter above approximately 500 nm, the movement governed by gravitation and impaction becomes important. The gravitational force will make large particles settle in the surrounding gas. When a particle has a diameter that is much larger than the distance between surrounding gas molecules, the gas can be considered as a continuous fluid. The gravitational pull on a particle is dependent on the difference between the density of the surrounding gas and the particle itself. Furthermore, the gravitational force is proportional to the particle mass. The terminal settling velocity is the velocity at which the opposing drag force exerted by the surrounding medium equals the gravitational force. (Kulkarni, Baron & Willeke, 2011)

It is often convenient to use what is called the aerodynamic diameter when investigating particle motion for micrometer sized particles. The aerodynamic diameter is the diameter of a unit-density spherical particle that has the same settling velocity as the particle in question. For particles above 1 µm, the slip correction factor is approximately unity and thus the aerodynamic diameter, d_a, can be calculated as follows

$$d_a = d_p \left(\frac{\rho_p}{\rho_0}\right)^{1/2} \tag{2.3}$$

where $\rho_0 = 1000\ \mathrm{kg/m^3}$ is the standard particle density, ρ_p is the particle density and d_p is the particle diameter. As large particles will settle out faster than smaller ones, the gravitational force is very effective at removing large particles from the surrounding gas. (Kulkarni, Baron & Willeke, 2011)

Furthermore, large particles tend to also be effectively removed from an air stream by forcing the gas to make an abrupt bend. This process is called inertial impaction. When large particles are approaching an obstacle (the bend) they are unable to follow the airstream because of their large momentum. Thus, the large particles proceed in the original direction due to their inertia and deposit on the surface of the obstacle. (Hinds, 1999)

2.1.2 **Particle Types for Lung Deposition Measurements**

When studying respiratory tract deposition, it is of outermost importance to use a non-toxic substance for aerosolization. Furthermore, it is advantageous to use a monodisperse and non-hygroscopic aerosol to obtain a narrow size distribution of a known size for both inhalation and exhalation. Additionally, the size is most easily determined for particles with a spherical shape. Different materials have been

studied in this thesis along with their potential advantages and disadvantages for studies of respiratory tract deposition.

2.1.2.1 Polystyrene Latex Spheres

Polystyrene latex (PSL) spheres are stable and non-toxic (Jakobsson et al. 2016). Furthermore, PSL sphere are hydrophobic and have a density of approximately 1.05 g/cm^3 at room temperature (Sigma Aldrich, 2016), which is close to standard density. Because of their advantageous characteristics, they are often used in calibrations of instruments that need particles with distinct size and very small standard-deviation. The PSL spheres are delivered suspended in water and can easily be diluted with ultrapure water and poured into a nebulizer. Previous studies, (i.e. Jakobsson et al. 2016) have used PSL nanoparticles for studying the lung deposition efficiency of airborne nanoparticles.

2.1.2.2 Silicon Dioxide Spheres

Monodisperse silicon dioxide (SiO_2) particles have high stability and are spherical. Furthermore, the particles are hydrophilic and have a density of 1.85 g/cm^3. SiO_2 spherical particles are delivered in aqueous solutions. (Micro particles, n.d.)

There are regulations for inhalation of crystalline SiO_2 and more specifically SiO_2 that has quartz structure. These regulations have a set limit for the maximum inhalation amount, 0.1 mg/m^3 (Arbetsmiljöverket, 2018). To investigate the structure of the SiO_2 particles that were purchased for this thesis, a few micrograms of these were sent to Arbets- och miljömedicin (AMM) in Örebro for knowing the percentage of quartz-structure in the SiO_2 spheres. There was no quartz structure in the SiO_2 spheres.

2.1.2.3 Lactose Particles

Lactose is commonly used as a carrier in dry-powder inhalers (DPI) used in the treatment of respiratory diseases (Pilcer, Wauthoz, & Amighi, 2012). Moreover, lactose is inert with both physical and chemical stability and thus is considered as toxicologically safe (Pilcer, Wauthoz, & Amighi, 2012). Furthermore, lactose has a rather low hygroscopic growth compared to for example inorganic salts. This is relevant since the relative humidity (RH) in the lungs is 99.5% (Rissler et al. 2017b) which lead to hygroscopic growing in size due to water uptake.

2.1.2.4 Salts

Salts such as sodium chloride (NaCl) and ammonium sulphate ($(NH_4)_2SO_4$) are easy to nebulize and can be used for evaluating the output and stability of different nebulizers. Furthermore, salts can be used as an initial “proof of concept” for evaluation of a fast CPC used for measuring the changes in number concentration during inhalation and exhalation. However, the drawbacks with salts are that they are hygroscopic and thus they will take up water and grow in the humid environment in the lung. Furthermore, salts are polydisperse.

2.1.3 **Generation of Aerosols**

There are various ways to generate aerosols. According to Willeke (1980), aerosol generators are classified either as dry powder or liquid droplet generators. Within the liquid aerosol generators, there are different types of droplet generators, i.e. mechanical dispersion of liquid and condensation of vapor (Willeke 1980). Mechanical dispersion of a liquid into droplets can be made by air nebulizers. Air nebulizers use compressed air to atomize a liquid into droplets. By letting air pass through a narrow tube, this emerging air will have a high velocity and create a low-pressure region at the exit of the tube. This low pressure will then result in liquid being pulled from the reservoir upwards through a feed tube. The result is an emission of small droplets that contains a certain number of particles. Large droplets will not be able to leave the nebulizer because these will impinge on the curved wall of the exit duct. In the set-up for this work, the emitted droplets are later dried by letting the aerosol pass through a tube with silica gel.

2.2 Measurement Techniques

2.2.1 **Scanning Mobility Particle Sizer**

A scanning mobility particle sizer (SMPS) is a measurement system for submicrometer particle size-distribution measurements (Kulkarni, Baron, & Willeke, 2011). A SMPS combines electrical mobility sizing using a differential mobility analyzer (DMA) with the counting of single particles, often using a condensation particle counter (CPC) (Kulkarni, Baron, & Willeke, 2011). Typically, this instrument can measure particles with a diameter of 5 - 500 nm and has a time resolution around 2 min. Faster versions of similar systems have been developed such as the fast mobility particle sizer (TSI, n.d.). In a SMPS system the DMA scans and select particles of a specific electric mobility by using different voltages (Kulkarni, Baron, & Willeke, 2011). These particles are then delivered to a CPC that provides particle size and concentration results (Ruzer & Harley, 2013). By knowing the charge of the particles, the size of the particles (electrical mobility size) can be determined. The SMPS often includes a bipolar charger in order to charge the particles according to a known charge distribution that is used for the data inversion.

2.2.2 **Condensation Particle Counter**

A CPC is an instrument for the detection of ultrafine particles (particles with a diameter of less than 100 nm). The CPC uses a condensation technique to make small aerosol particles grow into larger sizes which makes them spread light and become optically detectable. Three processes are involved in the CPC's measurement technique, i.e. supersaturation of working fluids (commonly butanol or water), particle growth by condensation of these vapors and lastly optical detection of the particles. (Kulkarni, Baron & Willeke, 2011)

There are various types of CPCs available on the market. One of the fastest being a so-called Mixing CPC (MCPC), Brechtel CPC Model 1720 which has an ultra-fast response time of 180 ms (Brechtel, n.d.). The MCPC uses two streams, one being the sample flow and the other a saturated flow, see Figure 2.2 (Brechtel, n.d.). These CPCs consist of three parts, a saturator with a reservoir of the working fluid (the liquid butanol bath), a mixing chamber (condenser) and a particle detector (optics block), see Figure 2.2 (Brechtel, n.d.). The main advantages with the MCPC are the fast time response and the minimal diffusional loss of aerosol particles (Kulkarni, Baron, & Willeke, 2011). Minimal diffusional loss of particles is made possible since the aerosol stream does not pass through the saturator and thus the MCPC has a short aerosol delivery distance (Kulkarni, Baron & Willeke, 2011)

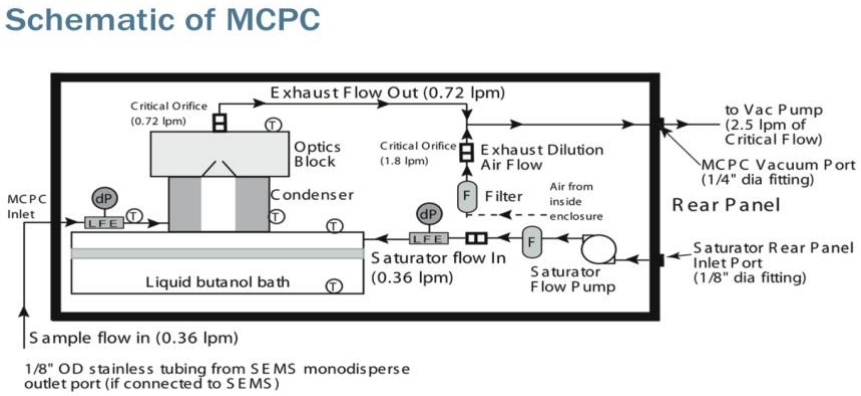

Figure 2.2 Schematic illustration of the Brechtel CPC Model 1720 (Brechtel, n.d).

2.2.3 **Aerodynamic Particle Sizer**

An aerodynamic particle sizer (APS) is a measurement device for particles with a diameter of 0.5 to 20 microns (TSI, 2006). The APS determines the aerodynamic size of a particle by measuring the particle velocity relative to the velocity of the air within an accelerating airflow (Kulkarni, Baron & Willeke, 2011). In the APS an aerosol nozzle flow is lead through an optical chamber and a sheath flow is used for accelerating the particles (TSI, 2006). Lighter (often smaller) particles will be

accelerated faster than heavier (often bigger) particles. Thus, larger particles will lag behind because of their higher inertia and have a longer transit time. The transit time is detected by diode lasers in the optical chamber (TSI, 2006). The sizing is however also density dependent. The lower density, the smaller aerodynamic size. The particle number concentration is then derived directly from the accumulator bin data and presented for each size (Kulkarni, Baron & Willeke, 2011). An APS has a minimum sample time of 1 s and a detection limit without coincidence for a maximum particle concentration of 1000 particles/cm^3 (TSI, 2006).

2.2.4 **Optical Particle Sizer**

An optical particle sizer (OPS) is a spectrometer that measures size-resolved particle concentrations optically. The measurement is made either by analysis of the light scattered by single particles or by the total scattered light. When particles pass through a well-defined measuring volume they are illuminated with white light and thus generate a light pulse (Palas, n.d.). The scattered light is detected by a photodetector and converted into an electrical pulse (Kulkarni, Baron & Willeke, 2011). The number concentration is derived from the count rate of these pulses whereas the size of the particles can be derived from the pulse height (Kulkarni, Baron & Willeke, 2011). The light scattered by an individual particle will depend on its specific shape, size and refractive index (Kulkarni, Baron & Willeke, 2011). The OPS of interest for the set-up of this work has a lower detection limit in particle size around 0.3 µm (Palas, n.d.). and a sample time around 10 ms. However, to assure coincidence-free measurements this specific OPS can only measure a maximum of 4000 particles/cm^3 (Palas, n.d.).

2.2.5 **Aerosol Mass Spectrometry**

The aerosol mass spectrometer (AMS) is a real-time measurement technique for the physicochemical characterization of aerosols. The AMS can determine chemical composition, size distributions as well as morphologies of the analyzed particles. The most widely used AMS is the one developed by Aerodyne Research, Inc. The AMS measures the non-refractory chemical speciation and mass loading using thermal vaporization as a function of particle size. Applications of the AMS in atmospheric aerosol studies are abundant, however, the instrument has not yet been deployed in other areas such as lung deposition and disease diagnosing. Possible, because of the rather large size of the instrument itself. Nonetheless, the possibility of real-time characterization of aerosols provided by the AMS poses a new and fascinating approach for analyzing aerosols in respiratory tract deposition studies. (Canagaratna, et al. 2007)

2.3 Respiratory Tract Deposition

2.3.1 **Anatomy of the Respiratory Tract**

The respiratory system is comprised of several different parts, see Figure 2.3, through which air passes through. First, the air is inhaled in the extra thoracic region via the nose or mouth and passes through the pharynx to the larynx. Subsequently, the air reaches the tracheobronchial region and flows through the trachea until it reaches a branching and enters the bronchi and further down the bronchioles. Ultimately the air reaches the alveolar region with the alveoli. (Widmaier, Raff & Strang, 2014)

The morphology of the respiratory tract influences the flow rate, pressure, direction and humidity of both inhaled and exhaled air or aerosol. These variating conditions and different tissues in the respiratory tract system influence both the sites and the rate of penetration and deposition of particles. Thus, the anatomy, its morphology and its dimensions are of outermost importance for understanding the deposition within the respiratory tract. (ICRP, 1994)

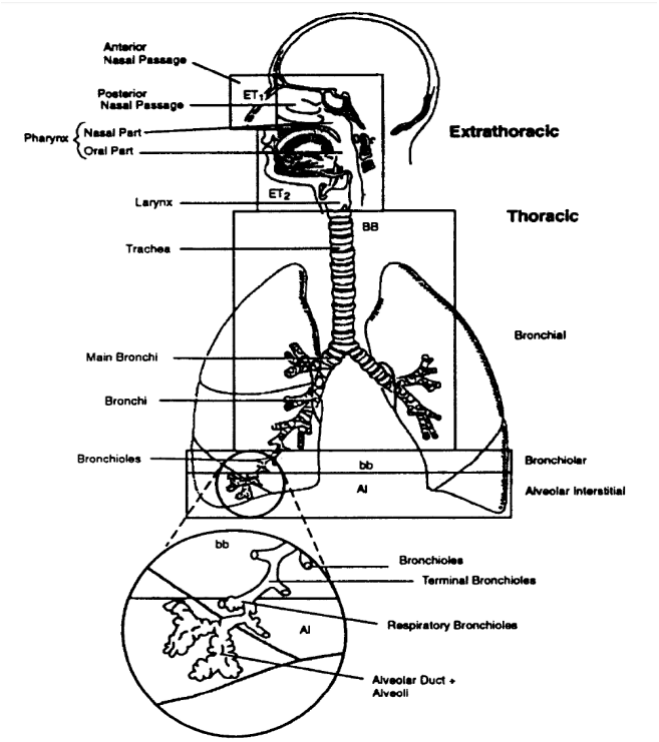

Figure 2.3 Anatomy of the human respiratory tract (ICRP, 1994).

2.3.2 **The Respiratory Cycle**

A respiratory cycle is a single sequence of inhalation and exhalation. Inhalation (inspiration) and exhalation (expiration) depend on the difference between the atmospheric pressure and the pressure in the lungs. The relationship between pressure and volume in a gas at constant temperature is described by Boyle's law:

$$P_1 V_1 = P_2 V_2 \tag{2.4}$$

where P_1 and V_1 is the pressure respectively the volume of system 1 and P_2 and V_2 is the pressure respectively the volume of system 2. (Widmaier, Raff & Strang, 2014)

The air volume entering the lungs during one inhalation or leaving during one exhalation is referred to as the tidal volume (V_t). The tidal volume at rest has an approximate value of 500 ml but depends on for example body size. A typical respiratory rate is around 12 breaths/min. Another important measure is the minute ventilation, which is the product of the respiratory rate and the tidal volume. (Widmaier, Raff & Strang, 2014)

2.3.3 **Deposition Fraction**

Since particle motion and transport is stochastic in nature, so is the deposition (Heyder et al. 1986). Therefore, deposition is defined as the mean probability of an inspired particle to be deposited (Heyder et al. 1986 and ICRP, 1994). The number ranges from 0 to 1, where 1 represents 100% deposition of all inhaled particles.

The deposition fraction is influenced by both physiological and anatomical parameters as well as the characteristics of the inhaled particles. The physiological and anatomical parameters of particular interest are the dimensions of the airways, the regional transit times and the flow rates. When it comes to particle characteristics, the size, shape and density of the inhaled particles will influence the deposition. (ICRP, 1994)

In Figure 2.4, the total deposition as well as the regional deposition, i.e. alveolar, tracheobronchial and head airways, have been plotted as a function of particle size. Figure 2.4 shows that larger particles (above 1 μm in diameter) deposit mainly in the head airways due to the high air velocity in the large airways that make the large particles deposit by impaction. Large particles deposit mainly by sedimentation in the tracheobronchial region and the alveolar region due to long residence times and smaller airway dimensions. The smallest particles will deposit in the head airway by diffusion even though the large dimension of these airways because the rate of

diffusion is very high. Deposition in the tracheobronchial region and alveolar region is also governed by a diffusional mechanism for small particles.

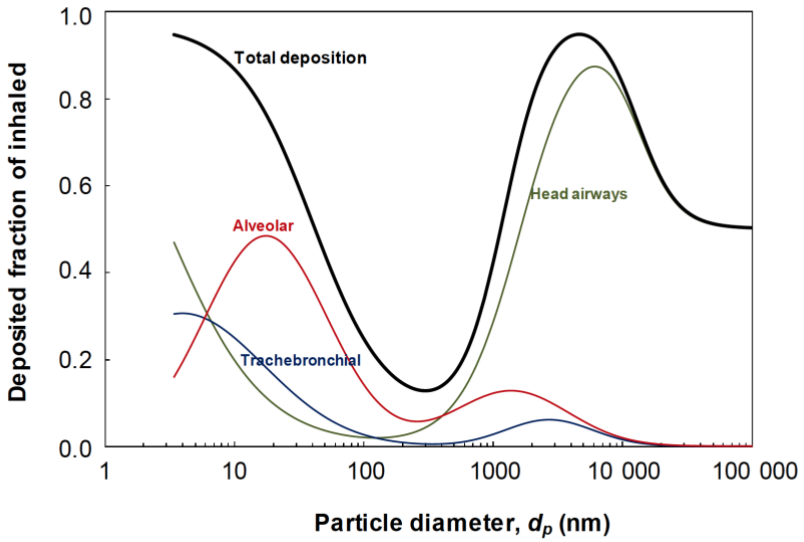

Figure 2.4 Deposited fraction of inhaled particles as a function of particle diameter. The curves have been generated from values in ICRP (1994) publication 66 and are representative for a sedentary person.

2.3.4 **Clearance Mechanisms**

The human respiratory tract has three main mechanisms for clearance of deposited particles, i.e. transportation to the gastrointestinal tract via the pharynx, absorption into the blood or transportation to the regional lymph nodes via lymphatic channels (ICRP, 1994). The epithelial cells of the upper part of the airways secrete mucus and macrophages capable of phagocytizing inhaled particles and pathogens (Widmaier, Raff & Strang, 2014). The inhaled particulate matter that gets deposited will stick to the mucus and later be moved by the cilia all the way up to the pharynx and consequently be swallowed (Widmaier, Raff & Strang, 2014). Moreover, particles that gets deposited further down, in the alveoli are removed by macrophages (Kopf, Schnedier & Nobs, 2015).

3 Methodology

In this chapter the methods that were used are presented with schematic overviews of the set-ups.

3.1 The Set-up

The set-up consists of three main modules: 1) aerosol generation, 2) inhalation system and 3) particle detection. A LabView program was developed to record the breathing flow pattern and detect both inhaled and exhaled particle concentrations. The set-up was developed after investigating previous set-ups in literature (i.e. Kim & Jaques, 2005; Löndahl et al. 2006; Heyder et al. 1973; Löndahl et al. 2014; Jakobsson et al. 2016; Rissler et al. 2017b and Lin et al. 2019). By first focusing on the desired functionalities of the set-up it was possible to use these as a foundation from which the required specifications could be developed. The functionalities were then matched to the corresponding instruments that would fulfill the desired functionality, e.g. one critical functionality being time resolution in each breath for particle concentration measurements, and the corresponding instrument that needs to be implemented is a fast OPS or CPC. The developed requirements have been listed in Appendix A.

Several schematic sketches of potential set-ups were then made and discussed together with the supervisors. The most essential parts used for different measurements within respiratory tract deposition were listed together with their functionalities. There were a few iterations with different schematic sketches before deciding on the selected set-up. An inventory list was made to facilitate for new purchases and to see what instruments could be provided directly by the Aerosol Lab. Later, the new purchases were made by the supervisor. The tubes needed for the breathing zone was designed in SolidWorks and later 3D printed at Ingvar Kamprad Designcentrum (IKDC).

3.1.1 **Aerosol Generation**

The initial tests for the aerosol generation were carried out to choose an appropriate nebulizer for the final set-up. First, an output comparison was made using ammonium sulphate for 4 different nebulizers. Secondly, the selected nebulizers were tested with larger particles, namely SiO_2 with an aerodynamic diameter of 2 µm, for a longer period of time and at various flow rates. The goal was to reach a concentration of 1000 - 3000 particles/cm^3 and have a steady and continuous generation of aerosol throughout 15-30 minutes.

3.1.1.1 Output Comparison of Nebulizers

A set-up was prepared as illustrated in Figure 3.1. With a radioactive source (KF10) placed inside the DMA (TSI, Model 3071). A second radioactive source was placed before the mixing chamber. The SMPS system (DMA TSI, Model 3071 and CPC TSI, Model 3775 coupled in series) used a sheath flow of 3 liters per minute (lpm), an aerosol sampling flow of 0.3 lpm and a sampling time of 135 s. The APS (TSI, Model 3321) had a flow of 0.9 lpm and a sampling time of 5 s. Both the SMPS and the APS was connected to the same computer. The generation tests were all carried out with ammonium sulphate, which was weighted (m = 0.20667 g) and mixed in 500 ml of purified water. Three different types of nebulizers were tested, two different ones (no. 1 and 2) requiring larger solution volumes (~1 dl) and two small ones (no. 3 and 4) requiring only <10 ml of the particle solution.

When testing the nebulizers, no dilution was used, i.e. the needle-valve to the dilution flow was closed, see Figure 3.1. The pressurized air flow was measured directly after a connected empty nebulizer. For the nebulizers no. 1 and 2 the same pressure was used resulting in different flowrates: 1.5 lpm (no. 1) and 2.4 lpm (no. 2). For the small nebulizers (no. 3 and 4) which do not work at high pressure the pressure needed to be decreased and consequently was decreased to reach approximately the same flow as nebulizer no. 2. (2.3 lpm). The output of the small nebulizer no. 4 was also investigated as a function of flow rate (1 to 3 lpm). The results were saved for later analysis in excel.

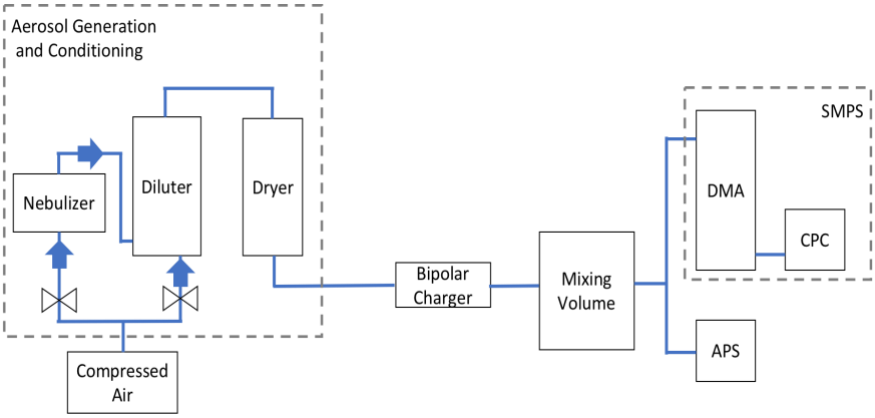

Figure 3.1 Schematic drawing of the set-up that was used for the aerosol generation tests. The aerosol is generated in the nebulizer and dried in the dryer. The aerosol passes through a bipolar charger before the mixing volume. The size distributions and number concentrations are then measured in the APS and the SMPS system in parallel.

3.1.1.2 Output and Stability

Two small nebulizers were tested (nebulizer 4 and 5) for stability and the desired output (above 1000 particles/cm^3). The set-up was prepared similarly as for the output comparison of nebulizers presented above, see Figure 3.1. The SMPS was set with a sheath flow of 3 lpm, a sampling flow of 0.3 lpm, a scan up time of 120 s and a retrace time of 15 s. The APS had a flow of 0.85 lpm and a sampling time of 5 s. The generation tests were carried out with SiO_2 in aqueous suspensions. There were 2 different dilutions of SiO_2 with purified water (diluted 1:2 and 1:4) that were tested for one of the nebulizers (no. 5), only 1:4 was tested for the other nebulizer (no. 4). The stability tests were carried out with a pressurized airflow of 3 lpm, which was measured directly before the nebulizer. The stock-solution of SiO_2 particles was a 0.5 wt.-% aqueous suspension of SiO_2 particles with a geometrical diameter of 1.7 µm. This corresponds to an aerodynamic equivalent diameter of ~ 2 µm, which can be calculated using Equation 2.3. The stock-solution was diluted as described above.

3.1.2 **Inhalation System**

3.1.2.1 Breathing Flow Module

The set-up to calibrate and test the breathing flow module is presented in Figure 3.2. First, a pneumotachograph was connected to a pressure meter which in turn was connected to a data acquisition card (DAQ) and connected to a computer. By using LabVIEW, a program was developed for reading the output of the pressure meter. To calibrate the pneumotachograph, specific flows were set and measured in series by an external flow meter as the pressure over the pneumotachograph was detected.

This allowed translation of the measured output signal (voltage) from the pressure meter into a corresponding flow.

The module for measuring the breathing flow, i.e. the pneumotachograph and connected pressure sensor, was considered to be one of the most critical parts of the set-up. The first pilot test was then used to build upon and expand with the same principle for the following measurement tools that needed to be monitored and read by the DAQ. Later, the LabVIEW program was expanded to also incorporate the calibration and save raw data (voltage) from the measurements.

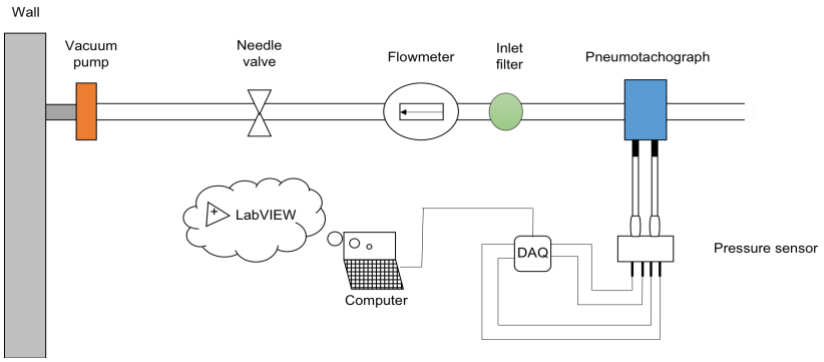

Figure 3.2 Schematic drawing of the breathing flow module that was used to calibrate the pneumotachograph. The flow was regulated by the needle-valve and read from the flowmeter. At the same time, the pressure sensor detects the difference in pressure over the pneumotachograph which yields a voltage signal that is read by the DAQ and sent to the computer.

3.1.2.2 Design

Initially, all dimensions of the fixed parts of the set-up, i.e. the pneumotachograph, mouthpiece, tanks, duck-valves and o-rings were measured. The additional tubings needed for the breathing zone was designed in SolidWorks with respect to the measured dimensions of the fixed parts. Test-rings were first designed and 3D-printed for accurate fitting. The internal volume of the two different branches was calculated using SolidWorks. Finally, the SolidWorks dimensions were updated and the final design (see Figure 3.3) was sent for 3D-printing at IKDC. Additionally, the inside of the tubings was sprayed with a conducting metal spray.

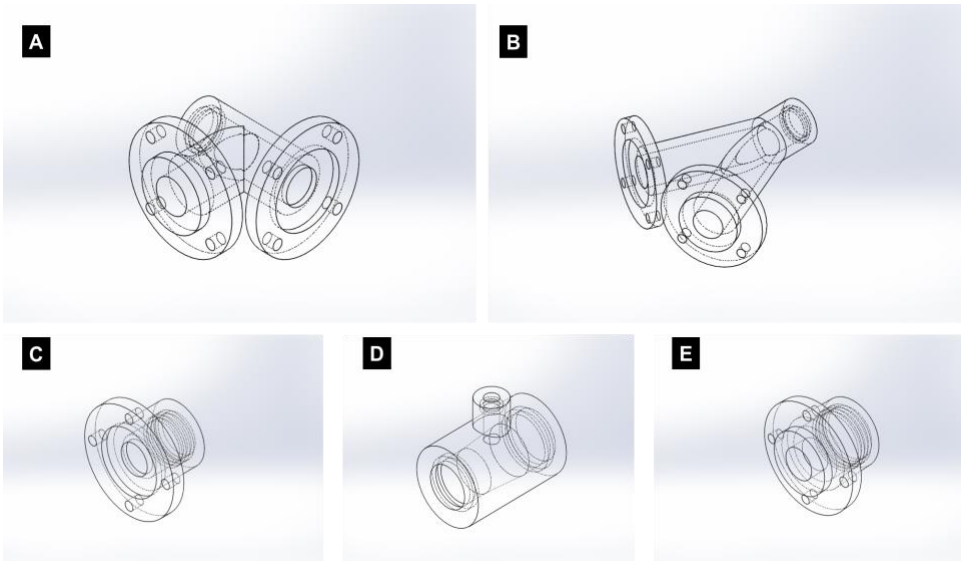

Figure 3.3 Final SolidWorks drawings. The figure shows A) the branch (in/out) with a 90° angle, B) the branch (in/out) with a small angle, C) duck-valve holder 2, D) the breathing tube and E) duck-valve holder 1.

3.1.3 **Particle Detection**

An OPS from Pallas (Welas 2000) was, after an investigation, considered to be the optimum choice for fast detection of large particles in the final set-up. However, this instrument was not available during the time and thus other instruments had to be used instead for proof of concept.

Several different instruments were used. In the above-mentioned aerosol generation tests, both an APS (TSI, Model 3321) and a SMPS system (DMA TSI, Model 3071 and CPC TSI, Model 3775 coupled in series) was used to obtain the size distribution and number concentration of the generated aerosol. For the assembled set-up a Brechtel CPC (Model 1720), with fast response time (180 ms) was used. Later, a DMA (TSI Model 3081) was placed right after the aerosol generation to create a monodisperse aerosol that enters the aerosol tank which was then measured by the Brechtel CPC (Model 1720) during inhalation and exhalation.

3.2 Characterization of the Complete Set-up

3.2.1 **The Four-Way Valve**

The set-up was prepared as illustrated in Figure 3.4. A four-way valve was connected to both pressurized air on one opening and vacuum on another, a third opening was left open and the fourth opening was connected directly into the set-up where the mouthpiece is supposed to be placed. The valve was switched manually over time, thus inducing abrupt changes in flow direction similarly to forced breathing. A Brechtel CPC (Model 1720) sampled the number concentration of the aerosol between the pneumotachograph and the inlet. Initially, measurements were made on room aerosol. The time lag due to the internal volume of the tubings was studied for the two different 3D-printed branches, a 90° angle and a small angle. Additionally, the response time of the CPC was studied for various flow rates through the system (i.e. 0, 3, 6, 9, 12 and 15 lpm).

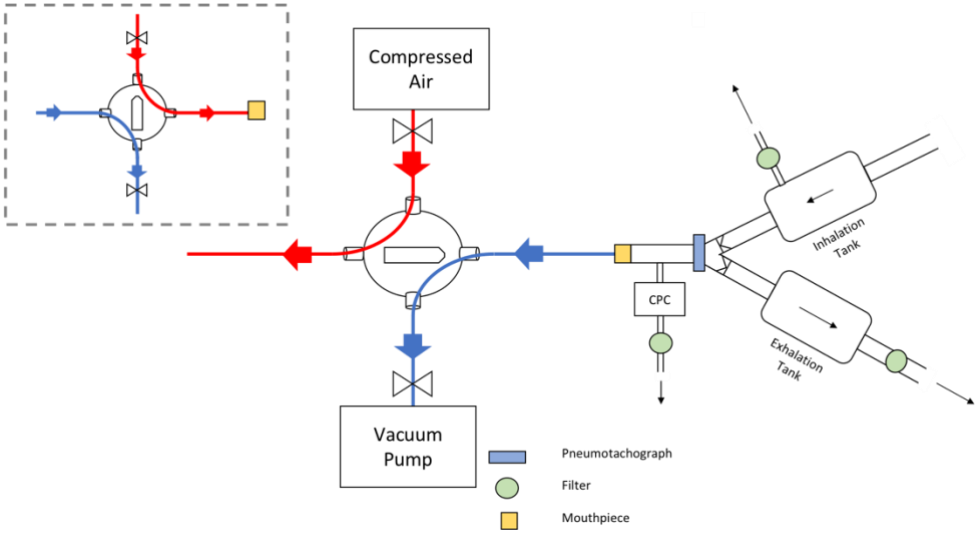

Figure 3.4 Schematic picture of the four-way valve set-up. Inhalation is simulated using a vacuum pump whereas exhalation is created using compressed air. Valve position and flow directions after switching the four-way valve is shown in the dashed box in the upper left corner of the figure.

3.2.2 **The Artificial Lung**

The set-up was prepared similarly as in Figure 3.4, but now an engine-driven cylinder (the artificial lung) was used to generate a realistic breathing flow pattern. The artificial lung was connected directly into the set-up where the mouthpiece is supposed to be placed. There were various algorithms tested, i.e. “LTH”, “Adult”

and “Child”. The “LTH” and “Adult” settings were very similar and simulated breathing of a healthy adult person, whereas the settings “Child” were simulating the breathing of a child, which is significantly different. Initially, the artificial lung was tested using the background room aerosol. To allow a more controlled concentration and particle size, the artificial lung was tested together with the aerosol generation of PSL particles with a diameter of 100 nm. The generated PSL particles were dried and pushed through a DMA set to only let particles of 100 nm pass through before entering the inhalation tank.

4 Results and Analysis

Chapter 4 presents the results of this study together with the analysis. The final set-up is presented here with a schematic sketch. Output in number concentration and size distributions are presented for the nebulizers, the 3D-printed parts are visualized and the calibration of the pneumotachograph is shown. Furthermore, results from the characterization of the complete set-up using the four-way valve and the artificial lung are presented.

4.1 The Set-up

Presented below in Figure 4.1 is a schematic drawing of the developed set-up. A continuous aerosol is generated and pumped into the inhalation tank. There is an opening in the inhalation tank to even out and maintain a constant pressure. A duck-valve is placed between the inhalation tank and the breathing system. This duck-valve will open during inhalation and close during exhalation. A pneumotachograph is placed after the duck-valve to measure the flow of aerosol during both inhalation and exhalation. The inhaled aerosol travel through a heated area, the breathing zone. The heating will minimize the condensation of particles. Furthermore, this zone was made with short and conductive tubing to minimize diffusive and electrostatic deposition. This will also result in a small dead space of the set-up. The breathing zone of the set-up was connected through 3D-printed tubings designed in SolidWorks which had been sprayed with metal spray on the inside. An ergonomic mouthpiece will let the subject breath spontaneously in and out, minimizing leaks by using a nose clip. The OPS will be placed in the heated area and during inhalation there will be a well-defined flow that goes through the OPS simultaneously as the subject is inhaling the same aerosol. When the subject starts exhaling, the duck-valve in front of the exhalation tank will open and the exhaled aerosol will travel both through the pneumotachograph and this duck-valve as well as to the OPS for measurement. All open ends have a filter to collect excess aerosol.

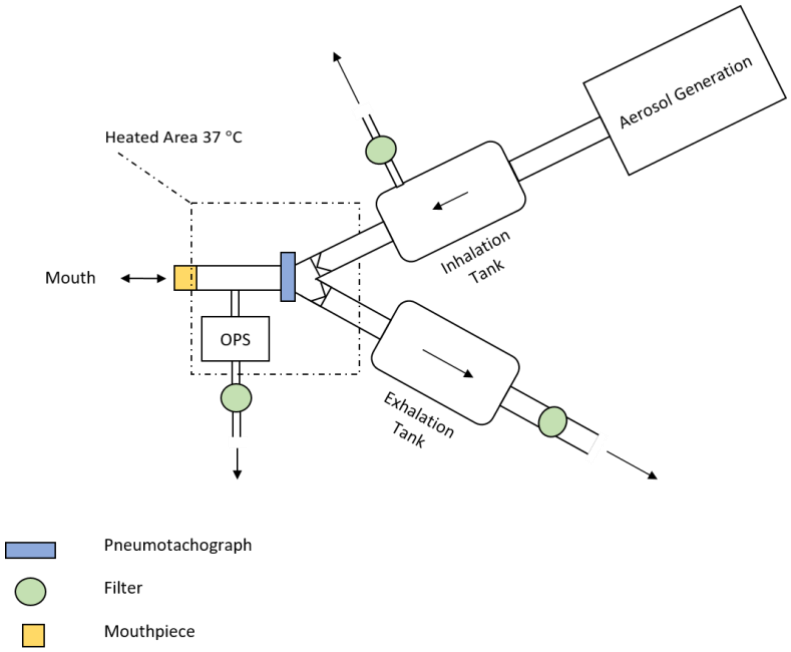

Figure 4.1 Schematic drawing of the final set-up of the system.

4.1.1 **Aerosol Generation**

4.1.1.1 Output Comparison of Nebulizers

The output comparison of the nebulizers was tested with salt particles, namely ammonium sulphate mixed with purified water. Nebulizer 2 showed the highest droplet output concentration (the highest generation of aerosol), followed by nebulizer 1 and lastly nebulizer 4, see Figure 4.2. Since it is hard to visualize the output of nebulizer 4 in the same diagram as no. 1 and 2, the droplet size distribution for no. 4 has been plotted alone in Figure 4.3. The results from nebulizer 3 is not presented because the nebulizer did not work properly and the output was too low.

The droplet size seems to increase with increasing output, i.e. in descending order nebulizer 1, 2 and 4. As this thesis initially aimed to use a monodisperse aerosol with an aerodynamic diameter of 2 µm, it was of interest to see which nebulizer that produced the largest droplet size. Nebulizer 2 created both the highest output concentration and also the largest droplet size. However, nebulizer 4 has the advantage of being of a better-suited container size (< 10 ml) and thus was a better choice for the purpose of this thesis since the monodisperse particles (PSL and SiO_2) are relatively expensive to purchase.

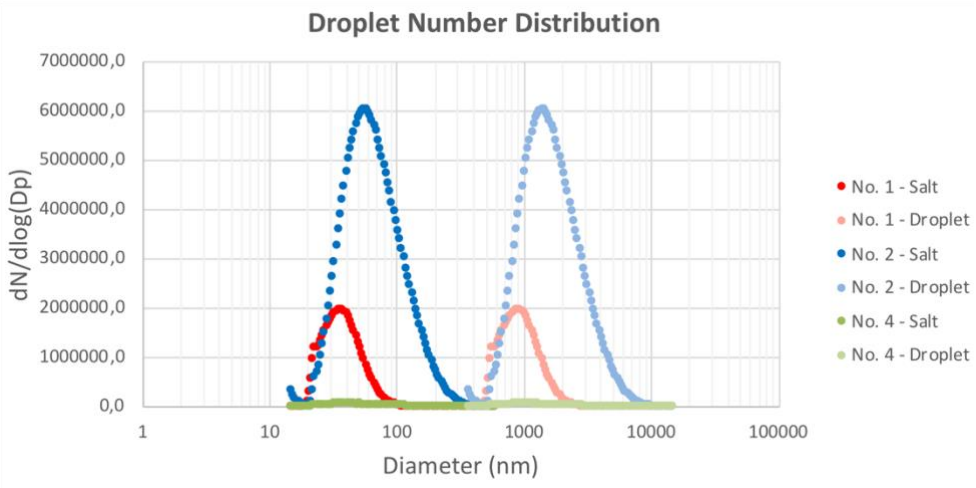

Figure 4.2 Output curves for nebulizer 1, 2 and 4 from the initial generation tests. The dark-colored left peaks are the measured dry salt distributions and the light-colored right peaks show the derived droplet size distributions.

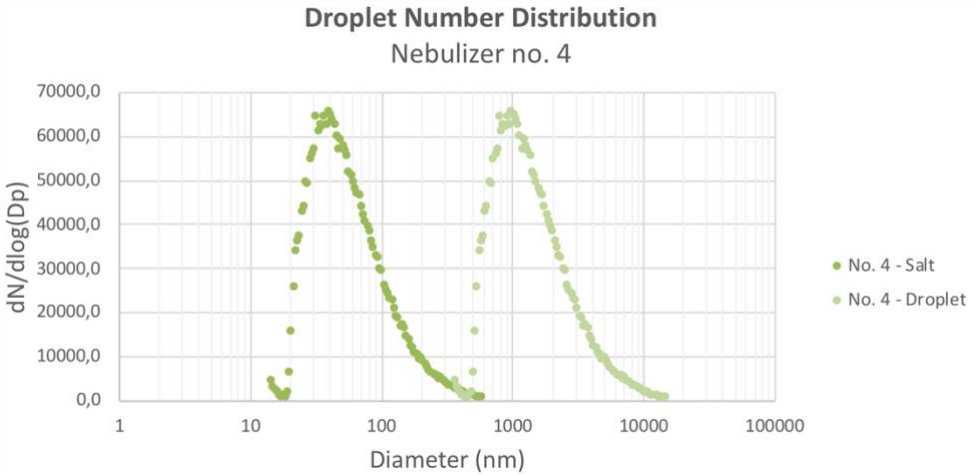

Figure 4.3 Output curves for nebulizer 4 from the initial generation tests. The left peak is the measured dry salt distribution and the right peak shows the derived droplet size distribution.

Note that in figure 4.2 and 4.3 the calculated droplet number distributions are shown together with the measured dry salt distributions. The droplet distributions have been calculated from the known salt concentration in the solutions that were nebulized. The calculations of the droplet number distributions do not compensate for any losses and thus potentially shows a larger concentration of the larger droplets which tend to impinge and not be able to leave the nebulizer in reality.

4.1.1.2 Output and Stability

The output (total number concentration) of nebulizer 5 was tested using SiO_2 and for a longer period of time, namely around 25-30 minutes to evaluate both the output of large particles as well as the stability of the nebulizer. As can be seen in Figure 4.4 the concentration measured by the APS is increasing initially during the first minute but then becomes rather stable. Additionally, Figure 4.4 shows that nebulizer 5 has the ability to generate the desired concentration of SiO_2 particles ~2 µm (above 1000 particles/cm^3) and thus was considered adequate nebulizer for the set-up.

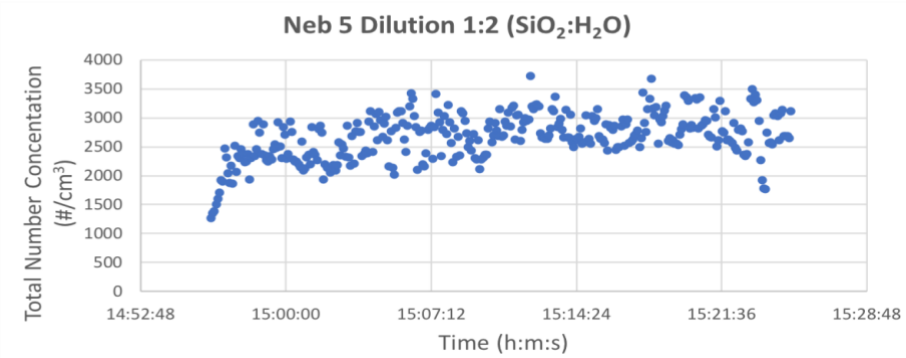

Figure 4.4 Total number concentration of particles > 700 nm for nebulizer 5 obtained from the APS data with a 1:2 dilution of SiO_2 in H_2O. The distribution > 700 nm was dominated by the 2 µm SiO_2 particles.

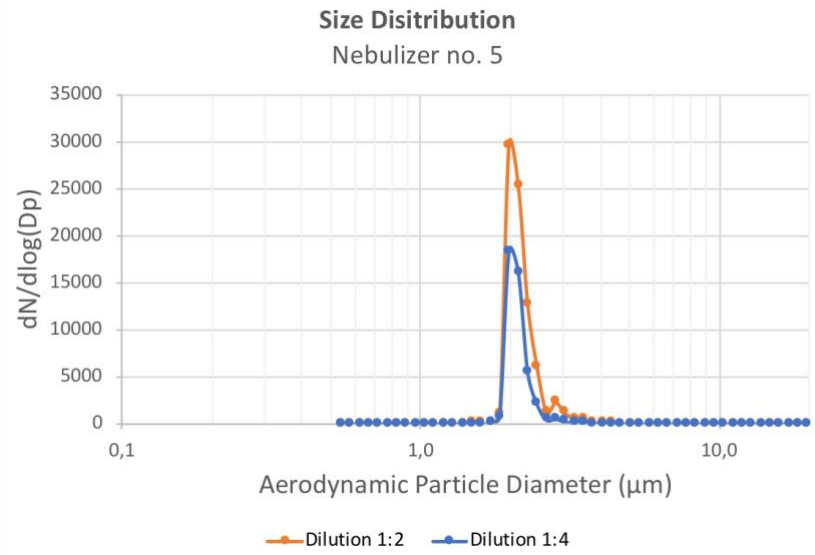

Figure 4.5 Obtained size distributions for dilution 1:2 (orange) and 1:4 (blue) using the APS data.

Figure 4.5 shows the size distributions obtained from the APS data for the two different dilutions tested on nebulizer 4. This figure shows distinct peaks at an

aerodynamic equivalent diameter of 2 µm, which corresponds to the 2 µm SiO_2 particles. Additionally, a very small peak is visible to the right of the orange curve. This small peak is assumed to be double-spheres. Both nebulizer 4 and 5 were tested with a 1:4 dilution of stock-solution of SiO_2 in ultrapure H_2O. The results can be found in Figure 4.6. Here one can see that nebulizer 5 has a larger output concentration than nebulizer 4. Furthermore, the concentration is lower for nebulizer 5 with a 1:4 dilution, (see Figure 4.6) compared to a 1:2 dilution (see Figure 4.4). Considering these results, nebulizer 5 with a dilution of 1:2 was found to be the most adequate choice for aerosol generation in the final set-up.

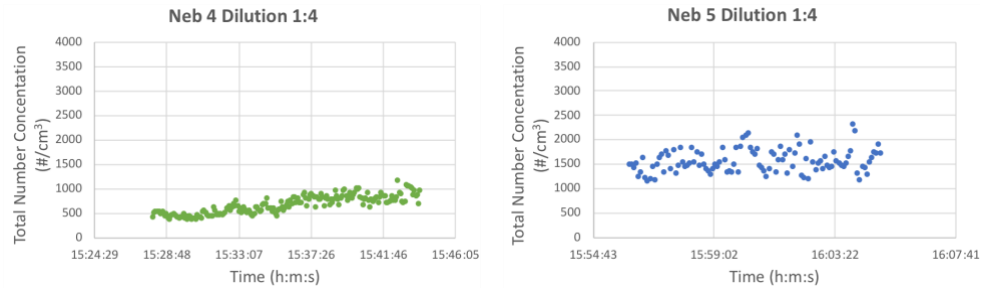

Figure 4.6 Total number concentration for nebulizer 4 and 5 obtained from the APS data with a 1:4 dilution of SiO_2 in H_2O.

The size distribution obtained from both the SMPS and APS data is presented together in Figure 4.7. The goal was to have a peak at an aerodynamic equivalent diameter of 2 µm corresponding to the 2 µm SiO_2 particles, which can be seen as the small orange peak in Figure 4.7. However, Figure 4.7 shows a much larger blue peak for smaller particle diameters. This is expected since there is always some background concentration generated by salt and other impurities in the water. Thus, to create a monodisperse aerosol with the SiO_2 particles one needs to use a selection method to eliminate the small particles. A virtual impactor could be used for this purpose. Alternatively, since the OPS will distinguish between particle size the OPS will allow to analyze the 2 µm particles. However, there is a risk that the smaller particles could interfere with the large if dominating the distribution measured by the OPS (> 0.3 µm).

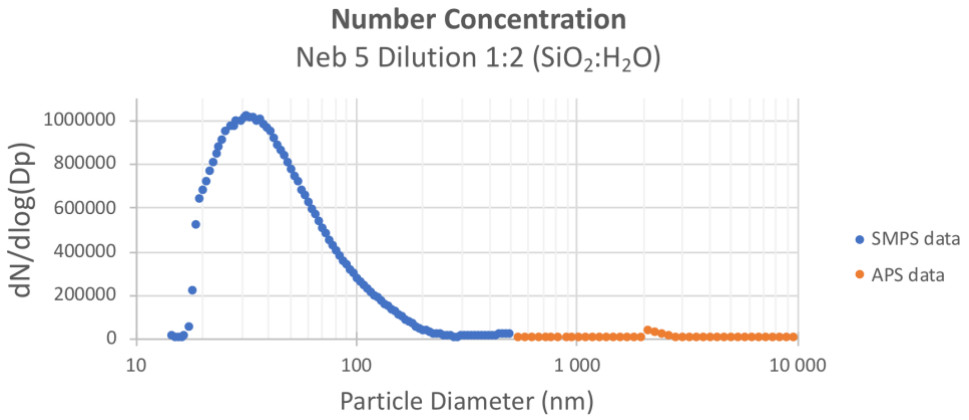

Figure 4.7 Obtained size distribution for nebulizer 5 with a 1:2 dilution of SiO_2 in H_2O using both SMPS and APS data

4.1.2 **Inhalation System**

4.1.2.1 3D-Printed Parts

The tubings for the inhalation system was designed in SolidWorks and later 3D printed. Additionally, the inside of the tubings was sprayed with a conducting metal spray. The resulting parts can be seen in Figure 4.8. Two different branches were made (see Figure 4.8 C and D). The two different branches have different advantages and disadvantages, depending on the assembly and point of measurement in of the set-up. The 90° angle will party work as an impactor and thus potentially can separate larger particles that do not follow the streamlines. However, since the aerosol is measured in the breathing zone this will not induce errors in the developed set-up. This would only be a potential disadvantage if the measurements were obtained from the inhalation and exhalation tank, as in previous studies, e.g. Rissler et al. 2017b. Moreover, the 90° angle branch has a much lower internal volume than the low angle branch, see Table 4.1.

Table 4.1 Calculated internal volume of the two branches.

	Internal Volume
90° Angle Branch	28 335 mm^3
Small Angle Branch	55 502 mm^3

Thus, the 90° angle branch constitutes a smaller instrumental dead volume which is a desirable design parameter for lung deposition studies since this volume will not be replaced with particles from the inhalation tank before being inhaled again. The duck-valve holders have been designed so that the duck-valve will be able to close and open as freely as possible.

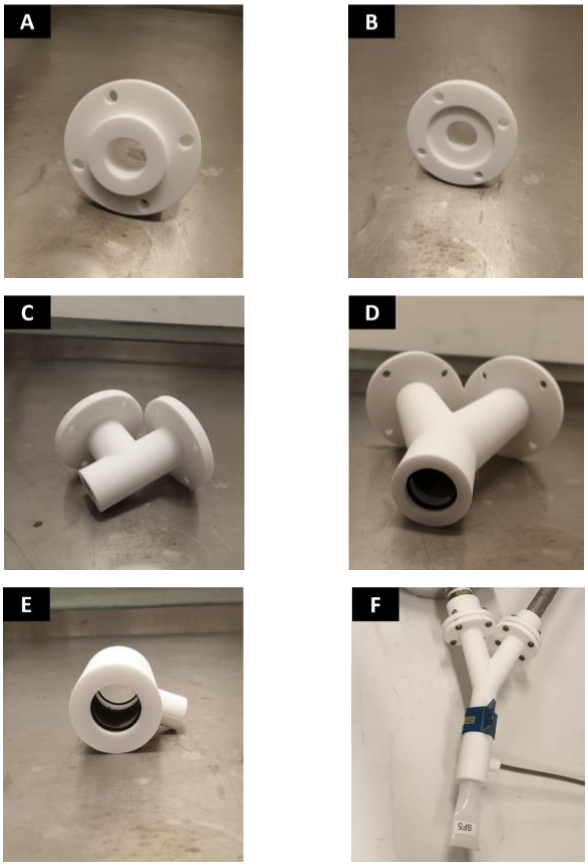

Figure 4.8 Pictures of the 3D-printed parts. The figure shows A) duck-valve holder 1, B) duck-valve holder 2, C) the branch (in/out) with a 90° angle, D) the branch (in/out) with a small angle, E) the breathing tube and F) the assembly of the parts.

4.1.2.2 Calibration of the Pneumotachograph

The initial calibration of the pneumotachograph was made using a 500 Pa sensor and resulted in a polynomial relation with degree 2 between the voltage output and the corresponding flow. The obtained data was plotted as flow vs. voltage. From the initial calibration curve generated for the 500 Pa sensor, it was evident that the 500 Pa sensor was not an optimum choice as the measured flows only gave rise to quite small pressure variations and thus only a small fraction of the voltage "window" was used (approximately 1.9 to 3.1 V of a window of 0 to 5 V). Thus, it was chosen to order a 125 Pa pressure sensor to obtain better voltage resolution and consequently better flow resolution.

The calibration curve for the 125 Pa pressure sensor showed better results. Now the voltages ranged from 1.4 to 3.6 V and thus provided better resolution for the measured flow. The calibration curve has been plotted in Figure 4.9. A polynomial

fit (deg 2) was made using Excel and the obtained relation was later used as a calibration curve for the pneumotachograph in the breathing-flow module.

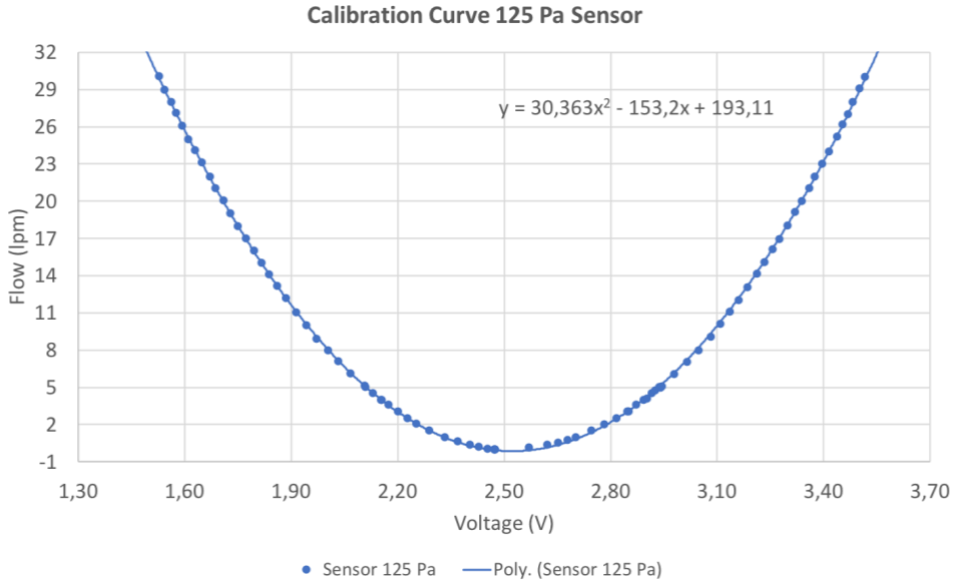

Figure 4.9 Calibration curve of the 125 Pa pressure sensor together with the pneumotachograph.

4.1.2.3 LabVIEW

A LabVIEW program was developed for reading the output of the pressure meter and later save the raw data (voltage) in a file. The first version was later built upon and expanded to measure and translate the voltage into flow and volume. Additionally, an already existing code for a CPC program was incorporated into the same LabVIEW code to enable accurate timing of the two programs that needed to be run simultaneously. The block diagram of the developed LabVIEW program for reading the pressure meter is found in Appendix B.

4.2 Characterization of the Complete Set-up

4.2.1 **The Four-Way Valve**

The four-way valve was switched manually over time from a vacuum flow sucking in air from the surrounding (inhalation) to particle free compressed air entering the system (exhalation). The flow direction of the vacuum flow (corresponding to an inhalation) was set as positive whereas the pressurized airflow was set to be negative, see Figure 4.10. The fact that the compressed air is particle free while the air pumped in from the surrounding contains particles allows the determination of

the time lags of the system. The abrupt changes in flow direction are evident in Figure 4.10. Similar patterns were obtained for flow rates of 6, 9, 12 and 15 lpm. However, the concentration does not change as abrupt during these abrupt changes in flow direction and thus shows some time delay due to the time it takes for the concentration to change, see Figure 4.10.

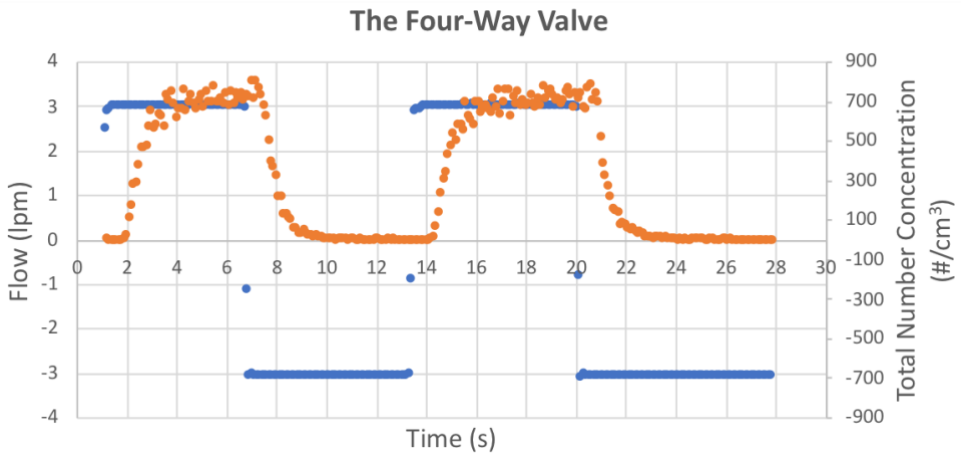

Figure 4.10 Flow pattern (blue) and total number concentration (orange) obtained for the low angle branch when switching the four-way valve manually from a fixed vacuum flow (3 lpm) to a fixed pressurized airflow (-3 lpm). The positive sign symbolizes inhalation whereas the negative sign represents exhalation.

To be able to compare the influence by the different flow rates and the two different branches, the number concentrations have been normalized with respect to their average concentration value when "high". The set-up was characterized by investigating the delay time and the smearing in the system. All raw concentration values have been normalized with respect to the average concentration when "high" and averaged over 4-5 runs for each flowrate. The smearing was obtained from the normalized plots, see Figure 4.11. The smearing was calculated from the rise time required for the response to rise from 10% to 90% of the final value when switching from pressurized air to vacuum. Whereas the smearing was calculated from the fall time required for the response to fall from 90% to 10% of the initial value when switching from vacuum to pressurized air. The delay time, the time lag of the system, was calculated from the time of a switching event, determined by the abrupt changes in flow-direction, until the concentration signal had reached 50% of its final "high" concentration value, see Figure 4.13.

4.2.1.1 Smearing

Figure 4.11 suggests an influence by the flowrate on the smearing effect. The rise and fall times of the two different branches and different flows are presented in Table 4.2. Furthermore, the influence by the flow-rate on the smearing is made even clearer in Figure 4.12 where the induced effect of smearing on the rise time of the signal has been plotted against the flow both for the 90° and low angle branch.

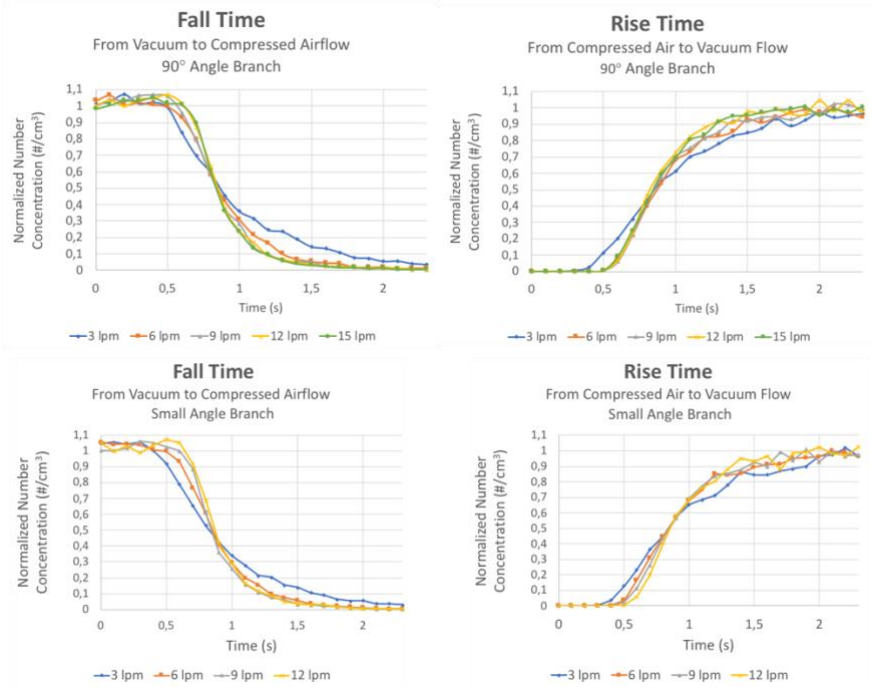

Figure 4.11 Smearing for different flows and branches.

Table 4.2 Smearing for different flow and branches. The fall and rise times have been obtained by studying Figure 4.11.

	Flow (lpm)	*From Vacuum to Compressed Airflow - Fall Time (s)*	*From Compressed Airflow to Vacuum - Rise Time (s)*
90° Angle Branch	3	1.15	1.15
	6	0.70	0.85
	9	0.55	0.75
	12	0.50	0.60
	15	0.50	0.70
Small Angle Branch	3	1.15	1.45
	6	0.70	1
	9	0.55	0.85
	12	0.55	0.7

The smearing induced time delay, fall time, seems to be decreasing with increased flow to a certain level (around 0.55 s at 9 lpm), for both branches, see Table 4.2. The lower level is likely set by the smearing delay due to the sampling to the CPC. The difference in smearing induced time delays of the two branches is not equally distinct as the flow dependence where higher flow corresponds to less smearing. Nonetheless, for lower flow rates, namely 3 lpm, there is a difference between the

two different branches, see Figure 4.12. Note that the case “from compressed air to vacuum” corresponds to the most system-relevant characterization.

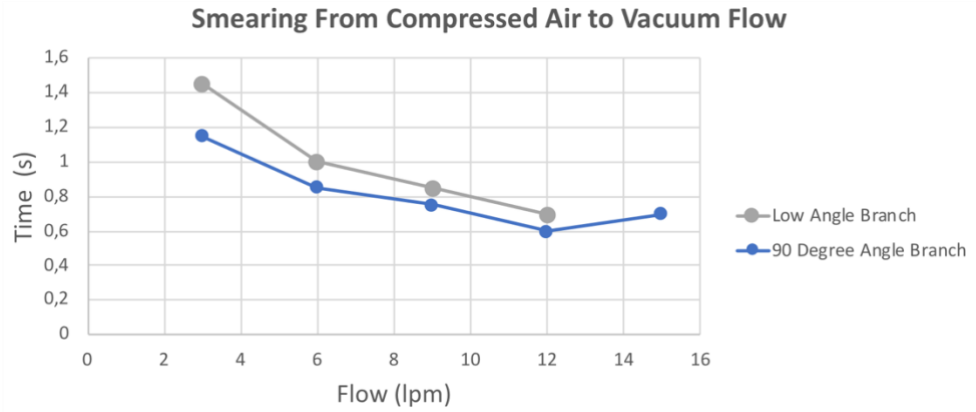

Figure 4.12 Comparison of the smearing when switching from compressed air to vacuum flow in two different branches for different flows.

4.2.1.2 Delay Time

Figure 4.13 shows an influence by the flow on the delay time of the system. For small flows, i.e. 3 lpm, the delay time is significantly larger than for the rest of the higher flowrates, i.e. 6, 9, 12 and 15 lpm, see Figure 4.13 and Table 4.3. The delay time seems to level off and reach approximately the same level for higher flow-rates, see Table 4.3 and Figure 4.14.

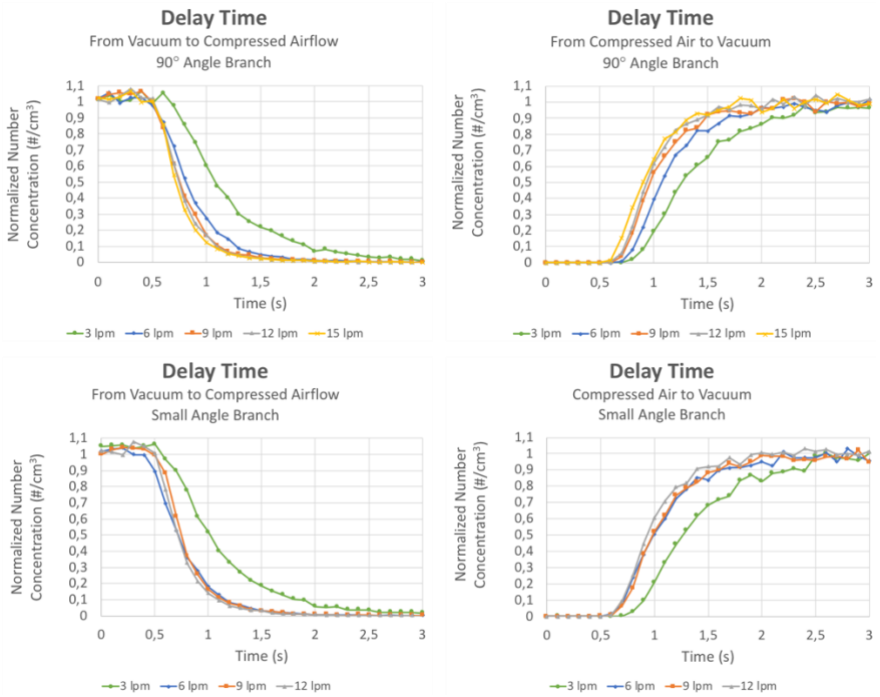

Figure 4.13 Delay time for different flows and branches.

Table 4.3 Delay time for different flows and branches. These delay times have been obtained by studying Figure 4.13

	Flow (lpm)	*From Vacuum to Compressed Airflow - Delay Time (s)*	*From Compressed Airflow to Vacuum - Delay Time (s)*
90° Angle Branch	3	1.1	1.25
	6	0.8	1.10
	9	0.75	0.95
	12	0.75	0.95
	15	0.75	0.90
Small Angle Branch	3	1	1.25
	6	0.75	1
	9	0.75	1
	12	0.75	0.95

Figure 4.14 does not show any significant difference in delay time when comparing the two different branches. However, there is a difference between the two different flow-directions, see Table 4.3, which is expected since the system is not symmetrical around the sampling point. The time lag when switching from compressed airflow to vacuum is the most interesting delay time for the set-up since this flow-direction represents the air entering through the system-parts of interest.

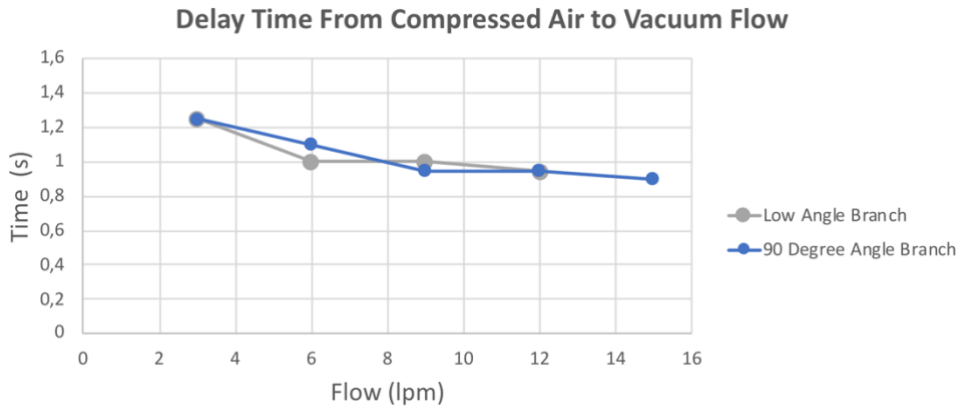

Figure 4.14 Delay time when switching from compressed air to vacuum flow in two different branches for different flows.

The observed delay times and smearing delays are assumed to be partly due to time lag when the air flows through the tubes in the inhalation system and can be accounted for by adjusting the lag-time of the raw number concentration data accordingly. The average value of the delay times for the 90° angle branch was calculated as 0.93 s, to be used for adjustment later on in this thesis. However, the real delay is flow dependent and in a later phase a more complex correction should be applied. The time lag was expected to be smaller for the 90° angle branch because of its smaller internal volume. Furthermore, the time lag and smearing delay may also be due to the sampling to the CPC. This is flow-independent for the inhalation and exhalation flow, while the first term is not.

4.2.2 **The Artificial Lung**

The artificial lung was used to simulate a more realistic breathing pattern compared to the abrupt changes generated by the four-way valve. Furthermore, a filter was placed between the artificial lung and the mouthpiece opening in the set-up. The filter was used to gain a more realistic pattern for the number concentration with exhalation through the filter being nearly zero particles/cm^3 as can be seen in Figure 4.15. In Figure 4.15 the artificial lung was tested together with the aerosol generation of PSL particles with a diameter of 100 nm.

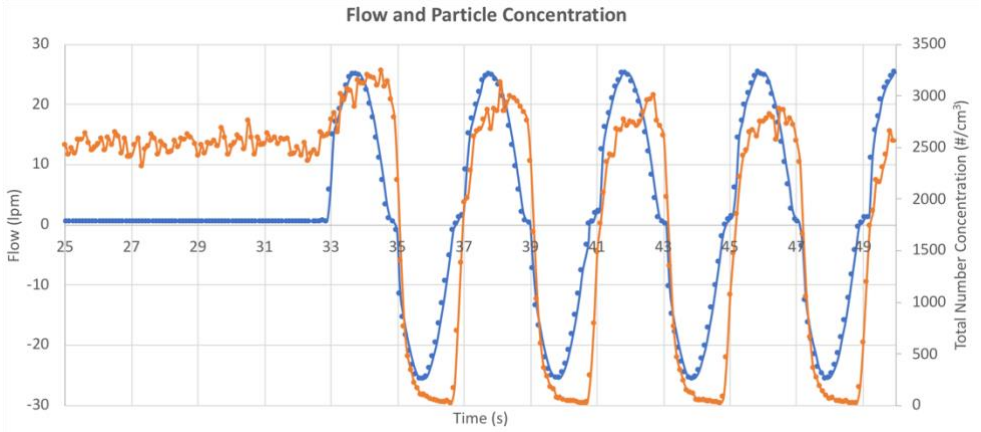

Figure 4.15 Flow pattern (blue) and particle concentration (orange) for settings "Adult" using the artificial lung and a filter. The concentration values have been adjusted according to the average value of the delay times (0.93 s) presented above.

The slow decline in the peaks of the total number concentration above in Figure 4.15 is due to that the aerosol generation only operates at 3 lpm and has been let to fill a 5 l inhalation tank before starting the experiment. When the artificial lung starts the 5 l tank is emptied faster than the new generation of aerosol and thus we get the breathing pattern presented above in Figure 4.15. However, what is not realistic in this pattern is the increase in number concentration at the onset of the simulated breathing, around 32 seconds on the time-axis. One would expect the number concentration to stay at a constant level during the inhalation and then fall during exhalation. The induced error might be because the CPC is sensitive to small changes in over and under pressure in the system. However, when the pressure was measured right before the CPC and compared to the normal pressure it was almost identical. Additionally, a flowmeter was added right between the CPC inlet and the sample tube entering into the breathing zone. The flowmeter showed a small oscillation in the sample flow during the operation of the artificial lung. This oscillation will inevitably induce errors in the total number concentration being measured as the CPC uses a fixed sample flow to calculate the total number concentration.

To be able to compare how accurate the obtained calibration curve for the pneumotachograph was, Figure 4.16 has been plotted. Figure 4.16 shows both the "LTH" settings for the artificial lung as well as measured flows for this program. The flow has been modified adjusted according to the previously mentioned average value of the delay times (0.93 s). The blue line in Figure 4.16 shows some artifacts for small flows, close to 0 lpm, when the artificial lung changes flow direction. This is assumed to be due to the control of the engine driven cylinder that drives the artificial lung and thus should not be considered as an error of the calibration of the pneumotachograph.

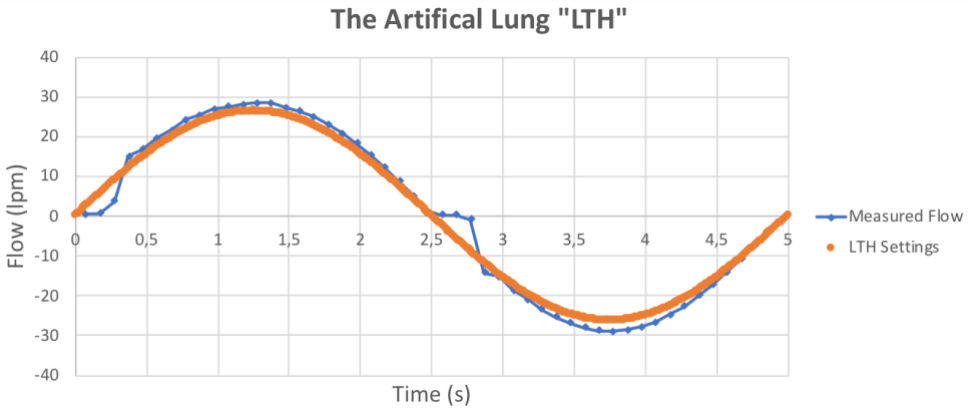

Figure 4.16 Measured flow pattern (blue) plotted together with the real settings for "LTH" (orange).

5 Discussion

In this chapter the analysis and results are discussed and validated. Additionally, limitations of the study are discussed. Lastly, a brief outlook is presented.

5.1 The Set-up

5.1.1 **Aerosol Generation**

5.1.1.1 Particle Types for Lung Deposition Measurements

There are various physicochemical properties that are of interest when studying aerosols and their respiratory tract deposition fraction. This thesis has considered characteristics such as size, hygroscopicity and hydrophobicity when deciding on suitable candidates for creating a monodisperse aerosol for the set-up. Studying how particles of a specific size deposits in the respiratory tract will provide a basic knowledge that can be applied to how air pollutants of the same size will be deposited, but also to how particles of other sizes will behave with respect to respiratory tract deposition, and especially the individual variation in lung deposition. Additionally, this thesis had to mitigate and accommodate the requirements of the available detection instruments which could fulfill the time requirements, i.e. the fast Brechtel CPC could only measure total counts. Thus, PSL particles with a diameter of 100 nm were used for the characterization of the set-up using the artificial lung and a filter. PSL is also a reasonable material for studies on humans. They have been used in previous studies, (i.e. Jakobsson et al., 2016). Their advantage lies in that they are monodisperse, easy to aerosolized and hydrophobic. However, PSL particles are expensive. This was one reason why SiO_2 was purchased instead. The SiO_2 particles are, as PSL particles, non-hygroscopic, and thus does not absorb water at 99.5% RH as in the lungs. Thus, they are considered equivalent to PSL. The toxicity of SiO_2 may however be questioned. Yet, the amorphous SiO_2 does not pose the same negative health affects as quartz. Lactose on the other hand is frequently used in medical inhalation studies and is considered to be non-toxic (Pilcer, Wauthoz & Amighi, 2012). The disadvantage with lactose

is that the particles are somewhat hygroscopic which is not ideal for respiratory tract deposition studies since they will grow in size in the lungs due to water uptake. Salts are even more hygroscopic, polydisperse and thus could only be used in this thesis for testing the output of the nebulizers, determining the smearing and delay time of the system and for showing proof of concept.

5.1.2 **Inhalation System**

5.1.2.1 Design

When designing the inhalation system several different aspects needed to be weight in. An alternative design that was considered was a flow-through system, as described by Löndahl et al. (2014) and Lin et al. (2019). This system would have the advantage of being compact and easy, with only a small breathing zone and spontaneous breathing would be possible even without duck-valves. However, the flow-through design would generate a lot of excess aerosol that is not inhaled, just wasted. This aspect is very undesirable because of the cost of the particles. Moreover, the excessive aerosol concentration would need to be filtered out when leaving the set-up, this filter might induce a larger pressure difference which would disturb the system.

Another design could be breathing induced aerosol generation, as in an inhalator where the aerosol is generated by the inhalation flow itself. A drawback of this system would be that it does not fully enable spontaneous breathing, but instead, a type of forced breathing. Additionally, it might be hard to minimize the delay for the aerosol to travel from the generation to the subject.

The final set-up, see Figure 4.1, that has been designed to minimize the particle losses in the breathing zone by using short tubing and a conductive inside material. The short tubing also provides a small instrumental dead space. Furthermore, the duck-valves allow for spontaneous breathing patterns and the heated zone will be used when studying human subjects to minimize condensation. The sampling is made through a probe that has been inserted vertically in the center of the breathing tube, this might induce turbulence and is not optimum from an isokinetic sampling point of view. In an isokinetic sampling procedure, the sampling probe is aligned parallel to the gas streamlines and the gas velocity entering the probe is equal to the free-stream velocity approaching the probe (Hinds, 1999). This procedure assures that a representative sample of aerosol enters the inlet of the sampling tube (Hinds, 1999). Failure of sampling in an appropriate way may result in a distortion of the size distribution and generate a biased estimate of the concentration (either a deficiency or an excess collection of large particles). Furthermore, it was not possible to characterize the set-up using an OPS because the instrument was not available. However, the Brechtel CPC (Model 1720) that was used did work as proof of concept with respect to the time resolution in each breath, still, with some

inconsistency, most likely created by the fluctuations in the sample flow. Similar studies, i.e. Lin et al. (2019), also found that high breathing flows induced fluctuations in the sampling flow of the CPC.

5.1.3 **Particle Detection**

Initially, this thesis aimed to study large particles and their lung deposition. For these measurements, it would have been ideal to use an OPS for measuring the number concentration. There are not really other options available for the larger particle sizes when having the time requirements that were set for the set-up. There is one OPS on the market fulfilling the requirements (Welas 2000). However, one option would have been to build an optical detection instrument from scratch, a stand-alone thesis in itself. The Brechtel CPC was then selected as the most promising detection instrument for the final set-up. A CPC however, only measures total number concentration, and thus required a DMA, with a set voltage selection, to be placed before the aerosol tank so that the aerosol entering the system was indeed monodisperse. The DMA, on the other hand, sets an upper limit on the selected particle diameters and thus what material that could be used.

5.2 Characterization of the Complete Set-up

When using the four-way valve for switching between compressed air and vacuum flow it became evident that the time lag and smearing in the system was rather large (around 1s) compared to the desired sampling time (around 0.1 s). To have a satisfactory time resolution in each breath for applications in lung deposition studies, it is of outermost importance to have a fast sampling time and to be able to compensate and adjust for the time delays. Fortunately, by observing the delay times and characterizing the system as a whole these time lags can be accounted for.

Another effect that needs to be accounted for is the smearing, both in the system itself and in the sampling tube to the CPC and within the CPC. The smearing occurs because of the laminar velocity profile in the tubes, and possibly some turbulence. The smearing in the sampling tube to the CPC does not have to do with the time lag induced by the internal volume of the inhalation system as a whole. However, the measured smearing is a sum of both the smearing in the inhalation system and the sampling to the CPC, as is the delay time. According to Collins et al. (2002), the additional mixing induced by external tubing is relatively small to that within the detector, if care has been taken to minimize the length of external tubing before entering the CPC. Correction for the CPC smearing can thus be made using inversion of the SMPS system and DMA transfer functions. There are two different techniques to remove the smearing effect presented by Collins et al. (2002), i.e. desmearing using a fitted curve or desmearing assuming exponential decay.

When it comes to the calibration of the pneumotachograph, see Figure 4.9, it can be observed that the left part of the curve follows the polynomial fit very well, whereas the right part of the curve is slightly off for lower voltage (corresponding to small flows in the exhalation direction, below 1 lpm). Figure 4.16 showed some artifacts for small flows, close to 0 lpm, when the cylinder in the artificial lung changes its engine driven direction. This is assumed to be because of the control of the engine driven cylinder and should not be an error from the calibration of the pneumotachograph.

5.3 Limitations

There were several measurement techniques that were initially of interest to use for the final set-up, i.e. a fast CPC, an OPS and an AMS. However, due to the limited amount of time and the availability of these instruments, the study was limited to only characterize the final set-up using the fast CPC. Additionally, in the schematic drawing of the final set-up, see Figure 4.1, there is a sketch of a "heated zone" which has not yet been built. There are two quite easy ways of building such a zone, i.e. by using a heating coil or a heat sink with a resistor combined with an insulating cover around the heated zone. Moreover, the losses in the mouthpiece before the sampling in the CPC could have been investigated further. Furthermore, the lactose was never aerosolized, but would have been a suitable aerosol to use for AMS measurements. Nebulization of lactose would however be similar to the nebulization of salts.

5.4 Outlook

Fast detection of particle concentration in the breathing zone is not as simple and straightforward as it might appear in thought. Various obstacles in the physical world need to be conquered before having a stable and satisfactory set-up for large-scale human respiratory tract deposition studies. The suggested set-up in this thesis could be improved quite easily to meet the requirements of human respiratory tract deposition measurements on a smaller scale. A key improvement that is needed is to have a stable and reliable measurement device that is not too sensitive of generated over and under pressure in the system.

In general, it is of outermost importance to continue researching the deposition of airborne particles in the respiratory tract to be able to understand the toxicity and the implications of exposure as well as how sensitive we are as individuals for the air pollutants in our surroundings.

6 Conclusion

This thesis aimed to build and test a novel set-up capable of detecting airborne particles in the breathing zone, with time resolution in each breath. A system was built and the first measurements for characterization of the final set-up were done.

The final set-up has been designed to minimize particle loss by using short tubing with a conductive material on the inside. The short tubing also provides a small instrumental dead volume. Furthermore, the duck-valves allow for spontaneous breathing and the heated zone will be used when studying real humans to minimize condensation. A fast CPC was used to characterize the final set-up for abrupt flow changes and also for a more realistic breathing pattern of an adult, generated by an artificial lung. The CPC showed a proof of concept for the time resolution requirements. However, there is a need for further investigation, due to CPC sample flow fluctuations during high inhalation and exhalation flowrates, before lung deposition studies on human subjects can be made. The most suitable aerosol material in the current set-up was found to be PSL particles, especially when characterizing the set-up.

For lung deposition studies on human subjects, further investigation is required to assure an appropriate particle material to be used. Additionally, a more stable and reliable measurement device with high time resolution would be a key improvement before using the suggested set-up in real lung deposition studies.

References

Arbetsmiljöverket. (2018). Hygieniska Gränsvärden. Available at: https://www.av.se/globalassets/filer/publikationer/foreskrifter/hygieniska-gransvarden-afs-2018-1.pdf Last Accessed: 2019-12-22

Brechtel. (n.d.). MCPC Mixing Condensation Particle Counter Model 1720. Available at: https://www.brechtel.com/wp-content/uploads/2014/10/Brechtel_Model_1720_MCPC_Brochure.pdf Last Accessed: 2020-01-04

Canagaratna, M. R., Jayne, J. T., Jimenez, J. L., Allan, J. D., Alfarra, M. R., Zhang, Q., Onasch, T. B., Drewnick, F., Coe, H., Middlebrook, A., Delia, A., Williams, L.R., Trimborn, A. M., Northway, M. J., DeCarlo, P. F., Kolb, C.E., Davidovits, P and Worsnop D. R. (2007). Chemical and microphysical characterization of ambient aerosols with the aerodyne aerosol mass spectrometer. in: *Mass Spectrometry Reviews*, Vol. 26, No. 2, pp. 185-222

Collins, D. R., Flagan, R. C. and Seinfeld, J. H. (2002). Improved Inversion of Scanning DMA Data, in: *Aerosol Science & Technology*, Vol. 36, No.1, pp. 1-9

Daigle C.C., Chalupa D.C., Gibb F.R., Morrow P.E., Oberdorster G, Utell M.J. and Frampton M.W. (2003). Ultrafine particle deposition in humans during rest and exercise. in: *Inhalation Toxicology* Vol. 15, pp. 539-552.

Heyder, J., Gebhart, J., Heigwer, G., Roth, C., and Stahlhofen W. (1973). Experimental studies of the total deposition of aerosol particles in the human respiratory tract in: *Aerosol Science*, Vol. 4, pp. 191-208.

Heyder, J., Gebhart, J., Rudolf, G., Schiller, C. F. and Stahlhofen W. (1986). Deposition of particles in the human respiratory tract the size range 0.005-15 m, in: *Aerosol Science*, Vol. 17, No. 5, pp. 811-825.

Hinds, W.C. (1999). Aerosol Technology: Properties, Behavior, and Measurement of Airborne Particles. Wiley. ISBN: 9780471194101

ICRP. (1994). Human Respiratory Tract Model for Radiological Protection. ICRP publication 66. Annals of the ICRP, Vol. 24 No.1-3

Jakobsson K.F., Hedlund J., Kumlin J., Wollmer P., and Löndahl, J. (2016). A new method for measuring lung deposition efficiency of airborne nanoparticles in a single breath. in: *Scientific Report* Vol. 6.

Kim C.S. and Jaques P.A. (2005). Total Lung Deposition of Ultrafine Particles in Elderly Subjects During Controlled Breathing. in: *Inhalation Toxicology* 17 pp. 387-399

Kopf, M., Schneider, C. and Nobs, S.P. (2015). The development and function of lung-resident macrophages and dendritic cells, in: *Nature Immunology*, Vol. 16, No. 1, pp. 36-44.

Kulkarni, P., Baron, P.A. and Willeke, K. (2011). Aerosol Measurements: Principles, Techniques and Applications. Wiley Inc. ISBN: 9780470387412

Lin C.W., Huang S.H., Chang K.N., Kuo Y.M., Wu H.D., Lai C.Y. and Chen C.C. (2019). Experimental Measurement of Regional Lung Deposition in Taiwanese. in: *Aerosol and Air Quality Research* Vol. 19, No. 4 pp. 832-839

Löndahl, J., Möller, W., Pagels, J.H., Kreyling, W. G., Swietlicki, E., and Schmid, O. (2014). Measurement Techniques for Respiratory Tract Deposition of Airborne Nanoparticles: A Critical Review in: *Journal of Aerosol Medicine and Pulmonary Drug Delivery* Vol. 27 No. 4, pp. 229-254

Löndahl, J., Pagels, J., Swietlicki, E., Zhou, J.C., Ketzel, M., Massling, A. and Bohgard, M. (2006). A set-up for field studies of respiratory tract deposition of fine and ultrafine particles in humans. in: *Aerosol Science* Vol. 37, pp. 1152– 1163

Micro particles. (n.d.). Silica particles (SiO2-R) in the size range 150 nm - 25 µm Available at: https://www.microparticles-shop.de/Monodisperse-Particles-for-Research-Purposes/Silica-particles-SiO2-R-in-the-size-range-150-nm-25-m:::1_6.html?language=en Last Accessed: 2019-12-22

Palas (n.d.). Aerosol sensor welas 2500. Available at: https://www.palas.de/en/product/download/aerosolsensorwelas2500/datasheet/pdf Last Accessed: 2020-01-04

Pilcer, G., Wauthoz, N., and Amighi, K. (2012). Lactose characteristics and the generation of aerosol. in: *Advanced Drug Delivery Reviews*, Vol. 64, No. 3, pp. 233-256

Rissler, J., Gudmundsson, A., Nicklasson, H., Swietlicki, E., Wollmer, P. and Löndahl, J. (2017a). Deposition efficiency of inhaled particles (15-5000 nm) related to breathing pattern and lung function: an experimental study in healthy children and adults, in: *Particle and Fibre Toxicology*, Vol. 14, No.1

Rissler, J., Nicklasson, H., Gudmundsson, A., Wollmer, P., Swietlicki, E. and Löndahl, J. (2017b). A set-up for Respiratory Tract Deposition Efficiency Measurements (15-5000 nm) and First Results for a Group of Children and Adults, in: *Aerosol and Air Quality Research*, Vol. 17, No. 5, pp. 1244-1255.

Ruzer, L. S. and Harley, N.H. (2013). Aerosols Handbook - Measurement, Dosimetry, and Health Effects 2nd edition, CRC Press Taylor & Francis Group, Florida. ISBN: 978-1-4398-5519-5 (eBook - PDF)

Sigma Aldrich. (2016). Product Information - Polystyrene Latex Beads. Available at: https://www.sigmaaldrich.com/content/dam/sigma-aldrich/docs/Sigma/Product_Information_Sheet/2/lb11pis.pdf Last Accessed: 2019-12-22

TSI. (n.d.). Fast Mobility Particle Sizer Spectrometer Model 3091. Available at: https://tsi.com/getmedia/474ab64a-1972-4c37-b0a8-16ae500e9592/Fast_Mobility_Particle_Sizer_3091_5001476_A4_WEB?ext=.pdf Last Accessed: 2020-01-04

TSI. (2006). Model 3321 Aerodynamic Particle Sizer Spectrometer Operations and Service Manual.

Widmaier, E.P., Raff, H. and Strang, K.T. (2014). Vander's Human Physiology - The Mechanisms of Body Function, McGraw-Hill Companies Inc. New York. ISBN: 978-0-07-337830-5

Willeke K. (1980). Generation of aerosols and facilities for exposure experiments. Ann Arbor Science Publishers Inc. Michigan. ISBN: 0-250-40293-9

World Health Organization, WHO (2018). Air Pollution. Available at: https://www.who.int/news-room/fact-sheets/detail/ambient-(outdoor)-air-quality-and-health Last Accessed: 2019-11-26

Appendix A Requirement Specifications

Set-up Requirements		
Functionalities		
Aerosol Generation	Inhalation and Exhalation	Size and Conc. Measurement
Monodispersity • Only one size of the particles (narrow size-distribution) **Continuous and steady flow** • Need to generate a steady flow of aerosol continuously during the experiment	• Enable spontaneous breathing • Do not want to "lose" a lot of aerosol (aerosol not inhaled should be minimized) • Minimize losses in the inhalation/exhalation tubes and systems • Minimize condensation of exhaled aerosol • Minimize leaks • Minimize pressure variations • Minimize or account for dead space • Monitor and detect breathing pattern/flow	• Enable time resolution in each breath (preferably frequency of 10 Hz --> 10 samples/s) • Accurate particle sizing • Detect both in/exhalation efficiently • Minimize "smearing" in time because of laminar flow
Components and Material		
Aerosol Generation	Inhalation and Exhalation	Size and Conc. Measurement
Monodisperse aerosol • PSL • Sugar particles (lactose) • SiO2-spheres **Nebulizators** • Depending on what conc., droplet size and particle size	**Enable spontaneous breathing** • Duck-valves **Minimize losses** • No "flow-through" system: Valves • Min. E-dep: Conducting Tubes • Min. Diff-dep: Short Tubes • Detect remaining losses - pump and measure via homemade cylinder **Minimize condensation** • Heat inhalation system + measurement devices - resistance + kylflåns or thermoelement • Supervise and maintain temp. and RH control - thermometer **Minimize leaks** • Test for leaks and use nose clip + good mouthpiece **Account for deadspace** • Measure dead space of the instrument (volume of tubes in breathing zone) • Lung dead space can be estimated 150-200 ml **Monitor breathing pattern** • Measure in/out-flow using pneumotachograph • "Artificial lung"/homemade cylinder	**OPS** • Size-range: 1 - 5 µm • Flow: 1 lpm • Time resolution: 0.1 s/sample **APS** • Size-range: > 1 um • Time resolution: 5 s/sample • Max conc: 3000 #/cm3 **CPC** • Size-range: 14nm - 500 nm • Time resolution: (120s scan + 15 s pause) /sample **SMPS** • Size-range: < 500 nm • Time resolution: (120s scan + 15 s pause) /sample

Appendix B LabVIEW Block Diagram